

A Numerical Comparison Between Quasi-Monte Carlo and Sparse Grid Stochastic Collocation Methods

Juarez dos Santos Azevedo^{1,*} and Saulo Pomponet Oliveira²

¹ CETEC-UFRB, Centro, 44380-000, Cruz das Almas-BA, Brazil.

² DMAT-UFPR, Centro Politécnico, 81531-980, Curitiba-PR, Brazil.

Received 26 January 2011; Accepted (in revised version) 23 September 2011

Communicated by Jan S. Hesthaven

Available online 28 March 2012

Abstract. Quasi-Monte Carlo methods and stochastic collocation methods based on sparse grids have become popular with solving stochastic partial differential equations. These methods use deterministic points for multi-dimensional integration or interpolation without suffering from the curse of dimensionality. It is not evident which method is best, specially on random models of physical phenomena. We numerically study the error of quasi-Monte Carlo and sparse grid methods in the context of groundwater flow in heterogeneous media. In particular, we consider the dependence of the variance error on the stochastic dimension and the number of samples/collocation points for steady flow problems in which the hydraulic conductivity is a lognormal process. The suitability of each technique is identified in terms of computational cost and error tolerance.

AMS subject classifications: 60H15, 65C05, 65C20, 65C20

Key words: Karhunen-Loève expansion, Monte Carlo, quasi-Monte Carlo, sparse grid.

1 Introduction

The simulation of natural phenomena are susceptible to uncertainties that may be present on initial conditions, boundary conditions, or material properties. A representative example is flow through porous media, where medium properties, such as hydraulic conductivity and porosity, are not precisely known due to the scarcity or limited accuracy of measurements.

A computational technique widely used for this purpose is the Monte Carlo method (MC). It entails generation of a large number of random realizations of input variables,

*Corresponding author. *Email addresses:* juarezsa@gmail.com (J. S. Azevedo), saulopo@ufpr.br (S. P. Oliveira)

solving deterministic flow simulations for each realization. This method is robust and conceptually simple, but requires intensive computational effort since the number of realizations needed to achieve statistical convergence is very large in general. On the other hand, other techniques for solving these problems have gained great attention in recent years: quasi-Monte Carlo (*QMC*) methods [8, 19, 21] and Sparse Grid (*SG*) collocation methods based on Smolyak quadrature [2, 4, 10, 30].

Traditionally, *QMC* methods are based on deterministic numerical integration [19] in analogy to the technique of Monte Carlo simulation. In *QMC*, pseudo-random sequences are replaced by deterministic, low discrepancy sequences. For these sequences, Koksma-Hlawka inequality yields a rate of convergence $\mathcal{O}(N_r^{-1} \log(N_r)^M)$, where N_r is the number of realizations and M represents the stochastic dimension [29]. Such an order of convergence is an improvement over the Monte Carlo method, which is $\mathcal{O}(N_r^{-1/2})$ [26].

From another standpoint, *SG* methods arise from the study of multivariate polynomial interpolation [24] and achieves fast convergence to the solution when it has sufficient smoothness in random space, offering high-order accuracy with convergence rate depending weakly on dimensionality. Both *QMC* and *SG* methods do not suffer from the curse of dimensionality, i.e., the exponential growth of the computational cost with the problem dimension, which is typical of tensor-product, multi-dimensional quadrature rules [22, 27, 30].

The purpose of this paper is to contrast *QMC* and *SG* methods. Previous studies in this direction were done by Bungartz et al. [6], who studied the potential of adaptive sparse grids for multivariate numerical quadrature. Their numerical results showed that the adaptive sparse grid is superior to *QMC* when the integrand is smooth. An analogous procedure is also adopted in context of asset-liability management (*ALM*) simulations. Gerstner et al. [12] show with different parameter setups how the accuracy of *MC*, *QMC* and *SG* methods depend on the variance and the smoothness of the corresponding integration problem and concluded that *QMC* and *SG* based on Gauss-Hermite quadrature formulas are often faster and more accurate than Monte Carlo simulation even for complex *ALM* models with many time steps.

However, such an analysis has not yet been reported for physical models involving spatially-correlated random input data, and this is the main motivation of the present work. Sparse grid methods have been thoroughly studied in this context and theoretical error estimates are available [23]. Efficient *QMC* implementations for these models have been recently proposed [14], though the error analysis is in a preliminary level (see also [33]). We focus our study in an elliptic equation that describes the fluid flow on a saturated, randomly heterogeneous porous media in which the hydraulic conductivity is a lognormal random field represented on the Karhunen-Loève expansion.

The paper is organized as follows. The next section introduces the model problem. The variational formulation of the problem and spatial discretization are given in Section 3. The *MC* and *QMC* algorithms are presented in Section 4. The sparse grid method is described in Section 5. Numerical experiments are discussed in Section 6.

2 Model problem

We consider a stochastic model governing the stationary motion of an incompressible Newtonian fluid in a isotropic and heterogeneous geology. Let D be a convex domain in \mathbb{R}^d ($d = 2$ or $d = 3$) with closure \overline{D} and let $(\Omega, \mathfrak{F}, \mu)$ a complete probability space, where Ω represents the set of outcomes, $\mathfrak{F} \subset 2^\Omega$ is a σ -algebra of events, and $\mu : \mathfrak{F} \rightarrow [0, 1]$ is a probability measure. The flow problem is stated as: Find the fluid pressure head $p : \overline{D} \times \Omega \rightarrow \mathbb{R}$ and Darcy seepage velocity $\mathbf{q} : \overline{D} \times \Omega \rightarrow \mathbb{R}^d$ such that, μ -almost everywhere in Ω ,

$$\begin{cases} \mathbf{q}(\mathbf{x};\omega) = -\kappa(\mathbf{x};\omega)\nabla p(\mathbf{x};\omega), & (\mathbf{x};\omega) \in D \times \Omega, \\ \nabla \cdot \mathbf{q}(\mathbf{x};\omega) = f(\mathbf{x},\omega), & (\mathbf{x};\omega) \in D \times \Omega, \\ p(\mathbf{x};\omega) = 0, & \mathbf{x} \in \partial D. \end{cases} \quad (2.1)$$

Here $\kappa(\mathbf{x};\omega)$ is the random hydraulic conductivity and ω represents a random event in the sample space Ω (see [3, 9] for a discussion on the existence and uniqueness of solutions). We assume that the log-conductivity $Y(\mathbf{x};\omega) = \ln(\kappa(\mathbf{x};\omega))$ is a second-order stationary Gaussian process and f is square integrable on $D \times \Omega$. From here on, angular brackets $\langle \cdot \rangle$ indicate mathematical expectation. In particular, we denote the mean of Y as $\langle Y \rangle$ and the fluctuation around the mean as $\tilde{Y} = Y - \langle Y \rangle$. We define the covariance between two points \mathbf{x} and \mathbf{y} as

$$C_Y(\mathbf{x}, \mathbf{y}) = \langle \tilde{Y}(\mathbf{x};\omega)\tilde{Y}(\mathbf{y};\omega) \rangle. \quad (2.2)$$

We suppose also that the geometric mean $\kappa_G = \exp(\langle Y \rangle)$ and variance σ_Y^2 are constant, and that $C_Y(\mathbf{x}, \mathbf{y}) = C_Y(\mathbf{x} - \mathbf{y})$. Moreover, we assume that the covariance is isotropic, i.e., $C_Y(\mathbf{x}, \mathbf{y}) = C_Y(r)$, where $r = |\mathbf{x} - \mathbf{y}|$ is the lag distance.

The numerical evaluation of statistical moments depends on the discretization of Eq. (2.1) in space and the stochastic domain. Once the problem is discretized in spatial domain, numerical methods may be applied in the stochastic domain. In the next section we will describe the spatial discretization by the finite element method.

3 Weak formulation

Let us approximate the log-conductivity $Y(\mathbf{x};\omega)$ by a truncated Karhunen-Loève (KL) expansion:

$$Y(\mathbf{x};\omega) \approx Y_M(\mathbf{x};\boldsymbol{\xi}(\omega)) = \langle Y(\mathbf{x};\omega) \rangle + \sum_{n=1}^M \sqrt{\lambda_n} \phi_n(\mathbf{x}) \xi_n(\omega), \quad (3.1)$$

where each realization $\omega \in \Omega$ defined on the probability space $(\Omega, \mathfrak{F}, \mu)$ is mapped to a random vector $\boldsymbol{\xi}(\omega) = (\xi_1(\omega), \dots, \xi_M(\omega))$ of independent and identically distributed Gaussian random variables, and whose eigenpairs (λ_n, ϕ_n) are obtained from the Fredholm integral equation of the second kind

$$\int_D C_Y(\mathbf{x}, \mathbf{y}) \phi_n(\mathbf{x}) d\mathbf{x} = \lambda_n \phi_n(\mathbf{y}). \quad (3.2)$$

The probability space $(\Omega, \mathfrak{F}, \mu)$ can be replaced by $(\Gamma, B(\Gamma), \rho(\xi)d\xi)$, where $\Gamma = \xi(\Omega) \subset \mathbb{R}^M$, $B(\Gamma)$ denotes the Borel σ -algebra on Γ , and $\rho(\xi)d\xi$ is the probability measure of the vector ξ [16].

The weak formulation of problem (2.1) consists of finding $p \in H_0^1(D) \otimes L_\rho^2(\Omega)$ such that

$$\int_D \langle \exp(Y_M(\mathbf{x}; \xi)) \nabla p(\mathbf{x}; \xi) \cdot \nabla \psi(\mathbf{x}; \xi) \rangle d\mathbf{x} = \int_D \langle f(\mathbf{x}; \xi) \psi(\mathbf{x}; \xi) \rangle d\mathbf{x}, \tag{3.3}$$

for any $\psi \in H_0^1(D) \otimes L_\rho^2(\Gamma)$, where $\langle \cdot \rangle$ is rewritten as $\langle \cdot \rangle = \int_\Gamma \cdot \rho(\xi) d\xi$.

3.1 Finite element approximation

The stochastic boundary value problem (2.1) now becomes a deterministic Dirichlet boundary value problem for an elliptic PDE with an M -dimensional parameter. It can be shown [23] that problem (3.3) is equivalent to

$$\int_D \exp(Y_M(\mathbf{x}; \xi)) \nabla p(\mathbf{x}; \xi) \cdot \nabla \psi(\mathbf{x}) d\mathbf{x} = \int_D f(\mathbf{x}; \xi) \psi(\mathbf{x}) d\mathbf{x}, \quad \forall \psi \in H_0^1(D), \tag{3.4}$$

almost surely in Γ .

Now let us perform the spatial discretization with the Galerkin method. In particular we choose $W_h(D) \subset H_0^1(D)$ as a standard finite element space of dimension N_h , which contains continuous piecewise polynomials defined on a regular triangulation \mathcal{T}_h that has a maximum mesh spacing parameter $h > 0$. It induces a semi-discrete approximation $p_h \in W_h(D) \otimes L_\rho^2(\Gamma)$ such that

$$\int_D \exp(Y_M(\mathbf{x}; \xi)) \nabla p_h(\mathbf{x}; \xi) \cdot \nabla \psi_h(\mathbf{x}) d\mathbf{x} = \int_D f(\mathbf{x}; \xi) \psi_h(\mathbf{x}) d\mathbf{x}, \quad \forall \psi_h \in W_h(D). \tag{3.5}$$

The fully-discrete approximation by the stochastic collocation method, the Monte Carlo method, and quasi-Monte Carlo methods can be written as

$$\int_D \exp(Y_M(\mathbf{x}; \xi^{(m)})) \nabla p_h(\mathbf{x}; \xi^{(m)}) \cdot \nabla \psi_h(\mathbf{x}) d\mathbf{x} = \int_D f(\mathbf{x}; \xi^{(m)}) \psi_h(\mathbf{x}) d\mathbf{x}, \tag{3.6}$$

for any $\psi_h \in W_h(D)$, where $m = 1, \dots, N_r$ and N_r represents the number of realizations. We can use $p_h(\mathbf{x}; \xi^{(1)}), \dots, p_h(\mathbf{x}; \xi^{(N_r)})$ to compute approximations of the probability distribution or statistical moments of $p_h(\mathbf{x}; \xi)$. These computations will depend on the choice of the vectors $\xi^{(m)}$ and their weights. Quasi-Monte Carlo and Sparse Grid algorithms are reviewed in the next sections.

4 Monte Carlo and quasi-Monte Carlo methods

The Monte Carlo method approximation for (3.5) is constructed by generating a pseudo-random set of normally distributed, independent samples $\xi^{(1)}, \dots, \xi^{(N_r)}$. For each realization $\xi^{(m)}$ we solve the deterministic problem (3.6) for $p_h(\mathbf{x}, \xi^{(m)})$. These realizations are equally-weighted; in particular, the expected value of $p_h(\mathbf{x}; \xi)$, defined by the M -dimensional integral

$$\mu_{p_h}(\mathbf{x}) = \int_{\Gamma} p_h(\mathbf{x}; \xi) \rho(\xi) d\xi \tag{4.1}$$

is approximated by the equally-weighted average

$$\mu_{p_h}^{MC}(\mathbf{x}) \approx \frac{1}{N_r} \sum_{k=1}^{N_r} p_h(\mathbf{x}; \xi^{(k)}). \tag{4.2}$$

Let us introduce quasi-Monte Carlo methods with the problem of multi-dimensional integrals such as (4.1). These methods approximate the integral of a given function f on the hypercube $[0,1]^M$ by an equally-weighted average of deterministic, uniformly-distributed points, i.e,

$$\int_{[0,1]^M} f(\mathbf{X}) d\mathbf{X} \approx \frac{1}{N_r} \sum_{k=1}^{N_r} f(\mathbf{X}^{(k)}), \tag{4.3}$$

whose deterministic points $\mathbf{X}^{(1)}, \mathbf{X}^{(2)}, \dots, \mathbf{X}^{(N_r)} \in [0,1]^M$ are chosen as elements of a low-discrepancy sequence. Several low-discrepancy sequences are extensively studied in [22]. In particular, the classical example of a low-discrepancy sequence is the unidimensional Sobol sequence, which is defined from a binary expansion of a natural integer n . In particular, for

$$n \equiv (q_m \cdots q_0)_2,$$

we have that $X_2^{(k)}$ is defined as

$$X_2^{(k)} = \sum_{j=0}^m \frac{q_j}{2^{j+1}}. \tag{4.4}$$

Fig. 1 shows the frequency distribution of 1000 normally-distributed pseudo-random numbers generated by Matlab[®] command *randn*(\cdot) and the inverse of the normal cumulative distribution function evaluated on 1000 terms of the Sobol sequence. We observe that the Sobol samples are better fitted to the normal distribution and require a small computational effort. However, this advantage holds if the integrand is smooth and the stochastic dimension M is small [20].

An s -dimensional generalization of this sequence, known as the Halton sequence, is given by $\mathbf{X}^{(k)} = (X_{p_1}^{(k)}, \dots, X_{p_s}^{(k)})$ where (p_1, \dots, p_s) are relatively prime integers, usually taken to be the first s primes. Even though standard Halton sequences perform well

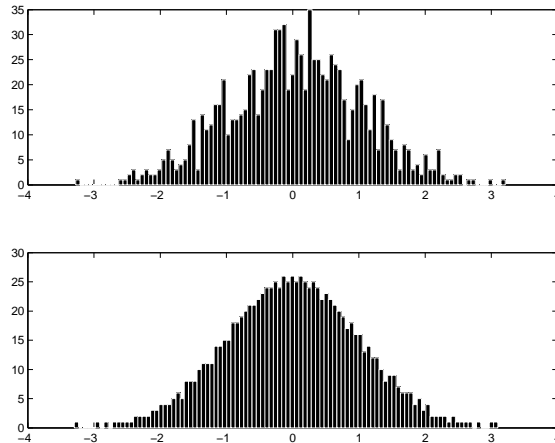


Figure 1: Frequency Histogram of 1000 samples of normally-distributed pseudo-random numbers (top) and the transformed Sobol sequence $\Phi^{-1}(\mathbf{X}^{(1)}), \dots, \Phi^{-1}(\mathbf{X}^{(1000)})$ (bottom).

in low dimensions, correlation problems have been noted in the sequences generated with higher primes [22]. In order to deal with this problem in our experiments we use the scrambled Halton sequence, which uses permutations of the coefficients used in the construction of the standard Halton sequence [17].

As in the experiments we deal with the estimation of integrals over unbounded domains with Gaussian weight, a change of variables is necessary in the expected value of the integral (4.1). In this case given an univariate standard normal cumulative distribution function $\Phi: \Gamma \rightarrow [0,1]^M$ we have:

$$\mu_{p_h}(\mathbf{x}) = \int_{[0,1]^M} p_h(\mathbf{x}; \Phi^{-1}(\mathbf{X})) d\mathbf{X}. \tag{4.5}$$

Thus the moments of (4.5) are approximated by

$$\mu_{p_h}^{QMC}(\mathbf{x}) \approx \frac{1}{N_r} \sum_{k=1}^{N_r} p_h(\mathbf{x}; \Phi^{-1}(\mathbf{X}^{(k)})), \tag{4.6a}$$

$$\sigma_{p_h}^{2,QMC}(\mathbf{x}) \approx \frac{1}{N_r} \sum_{k=1}^{N_r} (p_h(\mathbf{x}; \Phi^{-1}(\mathbf{X}^{(k)})) - \mu_{p_h}^{QMC}(\mathbf{x}))^2. \tag{4.6b}$$

5 Sparse grid algorithm

Let us review the stochastic collocation method and the sparse grid algorithm following the approaches [4, 31]. We have to properly select M -dimensional collocation points $\Theta_M = \{\boldsymbol{\zeta}^{(j)}\}_{j=1}^{N_r} \in \Gamma$. The standard stochastic collocation method constructs Θ_M from a tensor product of one-dimensional points. For each direction $i = 1, \dots, M$ we select m_i one-

dimensional collocation points $\Theta_1^i = \{\xi_i^{(j)}\}_{j=1}^{m_i}$ (for instance, Gaussian quadrature points) and define the interpolation operator \mathcal{I}_i as follows:

$$\mathcal{I}_i(f)(\xi) = \sum_{j=1}^{m_i} f(\xi_i^{(j)}) L_i^{(j)}(\xi), \tag{5.1}$$

where $L_i^{(j)}(\xi)$ are Lagrange polynomials satisfying $L_i^{(j)}(\xi_i^{(k)}) = \delta_{kj}$, $1 \leq k, j \leq m_i$. The interpolation operator \mathcal{I} of M -dimensional functions $f: \Gamma \rightarrow \mathbb{R}$ is defined by the following tensor-product formula:

$$\mathcal{I}(f)(\xi) = \mathcal{I}_1 \otimes \dots \otimes \mathcal{I}_M(f)(\xi) = \sum_{j_1=1}^{m_1} \dots \sum_{j_M=1}^{m_M} f(\xi_1^{(j_1)}, \dots, \xi_M^{(j_M)}) L_1^{(j_1)}(\xi_1) \dots L_M^{(j_M)}(\xi_M). \tag{5.2}$$

The fully-discrete approximation of Eq. (3.5) is then based on

$$p_h(\mathbf{x}, \xi) \approx p_h^{SG}(\mathbf{x}, \xi) = \sum_{m=1}^{N_r} \sum_{j=1}^{N_h} p_j^{(m)} \psi_j(\mathbf{x}) L_m(\xi), \tag{5.3}$$

where $L_m(\xi) = L_1^{(j_1)}(\xi_1) \dots L_M^{(j_M)}(\xi_M)$, $m = m(j_1, \dots, j_M)$, and $N_r = m_1 \times \dots \times m_M$. By approximating $\langle \cdot \rangle$ by a quadrature formula

$$\langle f \rangle \approx \sum_{m=1}^{N_r} w_m f(\xi^{(m)}), \tag{5.4}$$

Eq. (3.5) decouple and we arrive at (3.6). The full tensor-product space leads to the so-called *curse of dimensionality*, since N_r grows exponentially fast with the stochastic dimension M (see, for instance, [2]). In order to reduce the problem of curse of dimensionality and to expand the limits of practical computability we employ the sparse grid algorithm.

Let us introduce the vector $\mathbf{i} = (i_1, \dots, i_M) \in \mathbb{N}^M$ with cardinality $|\mathbf{i}| = i_1 + \dots + i_M$. The Smolyak interpolation formula [24] is

$$A_{q,M}(f) = \sum_{|\mathbf{i}| \leq q} \Delta_{i_1} \otimes \dots \otimes \Delta_{i_M}(f) = A_{q-1,M}(f) + \sum_{|\mathbf{i}|=q} \Delta_{i_1} \otimes \dots \otimes \Delta_{i_M}(f), \tag{5.5}$$

where $\mathcal{I}_0 = 0$ and $\Delta_i = \mathcal{I}_i - \mathcal{I}_{i-1}$, $i \in \mathbb{N}$. The integer parameter $q \geq M$ controls the order of interpolation. The Smolyak formula may also be written as a linear combination of tensor product formulas of the following type:

$$\mathcal{I}_{i_1} \otimes \dots \otimes \mathcal{I}_{i_M}(f)(\xi) = \sum_{j_1=1}^{m_{i_1}} \dots \sum_{j_M=1}^{m_{i_M}} f(\xi_{i_1}^{(j_1)}, \dots, \xi_{i_M}^{(j_M)}) L_{i_1}^{(j_1)}(\xi_{i_1}) \dots L_{i_M}^{(j_M)}(\xi_{i_M}), \tag{5.6}$$

where, in contrast with (5.2), the indices i_1, \dots, i_M are not restricted to the ordered sequence $\{1, \dots, M\}$. It can be shown (see [4] and the references therein) that the Smolyak formula (5.5) is equivalent to

$$A_{q,M}(f) = \sum_{q-M+1 \leq |\mathbf{i}| \leq q} \binom{M-1}{q-|\mathbf{i}|} \mathcal{I}_{i_1} \otimes \dots \otimes \mathcal{I}_{i_M}(f). \quad (5.7)$$

The set Θ_M of collocation points for the interpolation formula (5.7) is given by the sparse grid

$$\Theta_M = S_{q,M} = \bigcup_{q-M+1 \leq |\mathbf{i}| \leq q} \Theta_1^{i_1} \times \dots \times \Theta_1^{i_M}. \quad (5.8)$$

The Smolyak formula uses tensor products with a relatively small number of knots. Furthermore, exactness of one-dimensional interpolation is preserved for $M > 1$, in the sense that $A_{q,M}$ is exact when $q = M + K_{SG}$ for any polynomial of degree K_{SG} [4].

We employ the sparse grid implementation by Heiss and Winschel [15], in particular the Kronrod-Patterson rule for the normal probability measure $\rho(\boldsymbol{\xi})d\boldsymbol{\xi}$. This choice assures that, the one-dimensional nodal sets Θ_1^i of non-equidistant knots are nested, i.e., $\Theta_1^i \subset \Theta_1^{i+1}$, and subsequently $S_{q,M} \subset S_{q,M+1}$.

We choose $W_h(D)$ as the space spanned by the Lagrange polynomials associated to the points in $S_{q,M}$ and approximate $p_h(\mathbf{x}, \boldsymbol{\xi})$ as in (5.3). We also consider a quadrature formula in the form (5.4), according to the Kronrod-Patterson rule. Moreover, we have from (5.3) and (5.4) the following approximations of the mean and the variance of solution:

$$\mu_{p_h}^{SG}(\mathbf{x}) = \sum_{k=1}^{N_r} p_h^{SG}(\mathbf{x}, \boldsymbol{\xi}^{(k)}) \langle L_k(\boldsymbol{\xi}) \rangle = \sum_{k=1}^{N_r} p_h^{SG}(\mathbf{x}, \boldsymbol{\xi}^{(k)}) w_k, \quad (5.9)$$

$$\sigma_{p_h}^{2,SG}(\mathbf{x}) = \sum_{k=1}^{N_r} \sum_{j=1}^{N_r} (p_h^{SG}(\mathbf{x}, \boldsymbol{\xi}^{(k)}) - \mu_{SG})(p_h^{SG}(\mathbf{x}, \boldsymbol{\xi}^{(j)}) - \mu_{SG}) w_k w_j. \quad (5.10)$$

We should note that the accuracy of quadrature formulas depends strongly on the smoothness of the integrand [15].

6 Numerical results

In the following we present some experiments of two-dimensional flow in a saturated heterogenous porous media. We choose the flow domain and the log-conductivity mean as $D =]0,1[\times]0,1[$ and $\langle Y \rangle = 0$, respectively.

We study the dependence of the variance error on the stochastic dimension M and the number of realizations N_r . We employ the latter to compare the computational costs of SG and QMC. For SG the parameter N_r depends on the polynomial degree, the stochastic dimension, and the choice of the sparse grid (unlike QMC, in which this parameter is explicitly chosen). Table 1 shows the number of realizations of the SG algorithm with the

Table 1: Number of realizations for the Smolyak sparse grid algorithm with the Kronrod-Patterson rule.

	M=10	M=20	M=30	M=40	M=50	M=100
$K_{SG}=2$	21	41	61	81	101	201
$K_{SG}=3$	201	801	1801	3201	5001	20001
$K_{SG}=4$	1201	10001	34401	82401	162001	1314001

Smolyak sparse grid and the Kronrod-Patterson rule for some values of the probabilistic space M and the polynomial degree K_{SG} (see also Table 1 in [15]).

6.1 Lognormal pressure head

This example is a two-dimensional version of the experiment presented by Galvis and Sarkis [9]. Let us write the log-saturated hydraulic conductivity $Y = \log(\kappa)$ as

$$Y(\mathbf{x}, \omega) = \ll \omega, \phi \gg, \quad \ll \omega, \phi \gg = \sum_{n=1}^{\infty} \sqrt{\lambda_n} \phi_n(\mathbf{x}) \xi_n(\omega). \tag{6.1}$$

The source term $f(\mathbf{x}, \omega)$ is chosen such that the exact solution of (2.1) is given by

$$p(\mathbf{x}, \omega) = p(x_1, x_2, \omega) = \frac{x_1 x_2 (1-x_1)(1-x_2)}{4} e^{-\ll \omega, \phi \gg}; \tag{6.2}$$

that is,

$$f(x_1, x_2, \omega) = 0.25 x_2 (1-x_2) (2 - (1-2x_1) \ll \omega, \partial_{x_1} \phi \gg + x_1 (1-x_1) \ll \omega, \partial_{x_1 x_1} \phi \gg) + 0.25 x_1 (1-x_1) (2 - (1-2x_2) \ll \omega, \partial_{x_2} \phi \gg + x_2 (1-x_2) \ll \omega, \partial_{x_2 x_2} \phi \gg). \tag{6.3}$$

We choose the separable exponential covariance function $C_Y(\mathbf{x}, \mathbf{y}) = \sigma_Y^2 \exp(-(|x_1 - y_1|/\eta - |x_2 - y_2|/\eta))$. Here σ_Y^2 and η denote the variance and correlation length, respectively. The mean and the variance of the exact solution are given by

$$\langle p \rangle = \frac{x_1 x_2 (1-x_1)(1-x_2)}{4} e^{\sigma_Y^2/2}, \tag{6.4a}$$

$$\sigma_p^2 = \frac{x_1 x_2 (1-x_1)(1-x_2)}{4} e^{2\sigma_Y^2} - \langle p \rangle^2. \tag{6.4b}$$

Moreover (see, e.g., [32]), the eigenvalues and eigenfunctions associated with $C_Y(\mathbf{x}, \mathbf{y})$ are

$$\lambda_n = \tilde{\lambda}_i \tilde{\lambda}_j, \quad \phi_n(x_1, x_2) = \tilde{\phi}_i(x_1) \tilde{\phi}_j(x_2), \tag{6.5}$$

where $\{\tilde{\lambda}_i, \tilde{\phi}_i\}$ are the eigenpairs for the one-dimensional domain,

$$\tilde{\lambda}_i = \frac{2\eta\sigma_Y}{\eta^2\gamma_i^2 + 1}, \quad \tilde{\phi}_i(x) = \frac{\eta\gamma_i \cos(\gamma_i x) + \sin(\gamma_i x)}{\sqrt{(\eta^2(\gamma_i)^2 + 1)/2 + \eta}}, \tag{6.6}$$

and the index $n = n(i, j)$ is set to arrange the eigenvalues in decreasing order. The parameters $\gamma_1, \gamma_2, \dots$ are roots of the equation

$$(\eta^2 \gamma^2 - 1) \sin(\gamma) = 2\eta\gamma \cos(\gamma). \tag{6.7}$$

The exact solution (6.2) with $\sigma_\gamma = 1$ and $\eta = 0.1$ will be the target in comparison with QMC and SG methods based on KL expansion. The domain is uniformly discretized into 40×40 square elements.

Motivated by the error analysis in [23], we also consider the truncation error $\|\sigma_p^2 - \sigma_{p_M}^2\|$, where p_M is obtained by truncating the random input data. In particular, we truncate the operator (6.1) as follows:

$$\ll \omega, \phi \gg_M = \sum_{n=1}^M \sqrt{\lambda_n} \phi_n(\mathbf{x}) \zeta_n(\omega). \tag{6.8}$$

The corresponding solution p_M is

$$p_M(x_1, x_2, \omega) = \frac{1}{4} x_1 x_2 (1 - x_1) (1 - x_2) \exp(-\ll \omega, \phi \gg_M),$$

and the first two moments are

$$\langle p_M \rangle = \frac{x_1 x_2 (1 - x_1) (1 - x_2)}{4} \exp\left(\frac{1}{2} \sum_{n=1}^M \lambda_n \phi_n(\mathbf{x})^2\right), \tag{6.9a}$$

$$\sigma_{p_M}^2 = \frac{x_1 x_2 (1 - x_1) (1 - x_2)}{4} \exp\left(2 \sum_{n=1}^M \lambda_n \phi_n(\mathbf{x})^2\right) - \langle p \rangle^2. \tag{6.9b}$$

Fig. 2 depicts the comparison of head variance derived from exact solution and quasi-Monte Carlo methods with 100 and 1000 realizations considering the Halton and Sobol sequences. The QMC solution with $M = 10$ had a modest improvement from $N_r = 100$ to $N_r = 1000$. When the stochastic dimension is high, as illustrated by the solutions with $M = 100$ and $M = 400$, the variances obtained from 100 samples are far from having the smooth and even features of the target solution, but greatly improve with $N_r = 1000$.

Fig. 3 shows the profile curves of variance computed with the SG algorithm. These curves are smoother than the ones in Fig. 2, but the solutions given the SG algorithm underestimate the exact variance and depend on using a large stochastic dimension M to effectively decrease the error, as in QMC.

Fig. 4 shows the error in the L^2 norm of the variance as the stochastic dimension M varies from 10 to 50. The convergence of QMC is faster and it is comparable with SG with $K_{SG} = 4$, which needs a much larger number of realizations (Table 1). The truncation error has the same magnitude of the total errors, which suggests that this component dominates the total error of both methods. Moreover, the truncation error decreases very slowly with M due to the tensorial structure of the eigenpairs in (6.5).

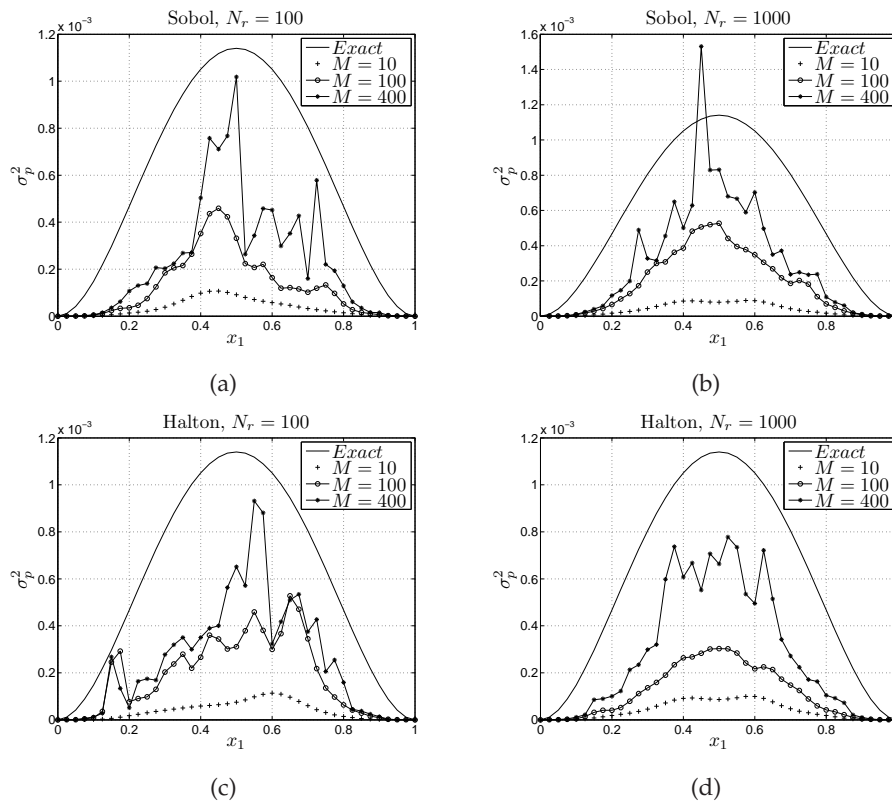


Figure 2: Cross sections of pressure head variance along the line $x_2 = 0.5$ for QMC with Sobol and Halton sequences.

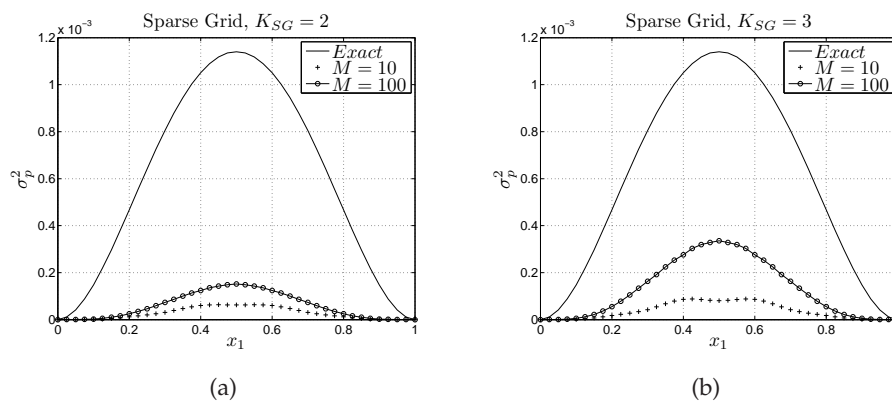


Figure 3: Cross sections of pressure head variance along the line $x_2 = 0.5$ for SG.

We present next the variance error of both methods with respect to the number of realizations N_r . Fig. 5 contrasts the variance errors of QMC with $M = 10, 100$ and 400 with the errors of SG with $K_{SG} = 2, 3, 4$. The dashed lines in Fig. 5 (left) connect variance errors with $M = 10$ and $M = 20$; these lines would be vertical lines in Fig. 4 (left) and show that

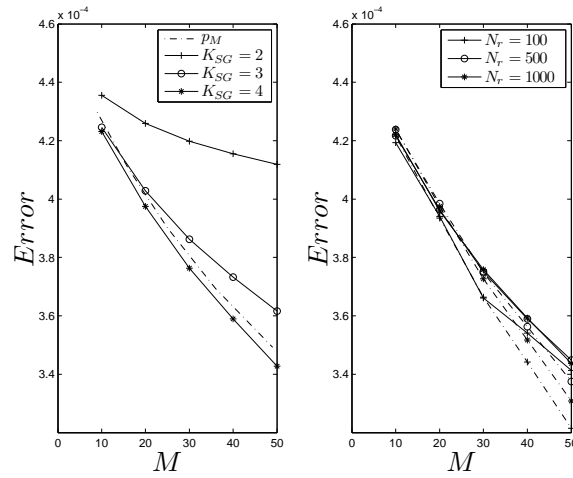


Figure 4: Error (on L^2 norm) of the variance with respect to stochastic dimension M . Left: SG and p_M ; Right: QMC with Halton (solid lines) and Sobol (dashed lines) sequences.

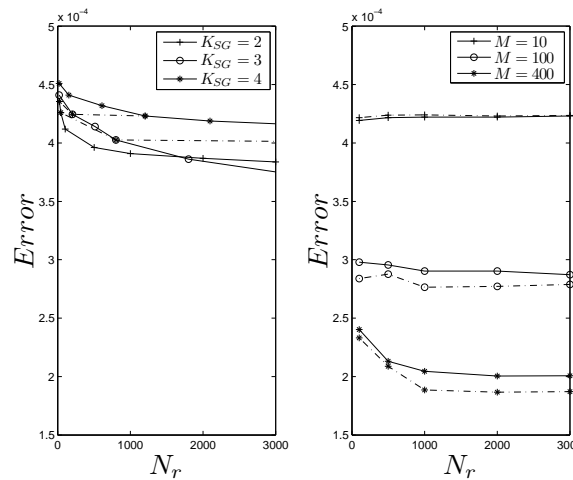


Figure 5: Error (on L^2 norm) of the variance with respect to the number of realizations. Left: SG (dashed lines connect variance errors with $M = 10$ and with $M = 20$); Right: QMC with Halton (solid lines) and Sobol (dashed lines) sequences.

the error decreases with the polynomial degree for a fixed value of M . QMC algorithms provide lower errors because they are able to handle $M \geq 100$ with a smaller number of realizations. Such values of M can be reached with SG with a similar number of realizations only if $K_{SG} = 2$, but this polynomial degree is not sufficient to approximate the exponential dependence of the solution on $Y(x, \omega)$. Furthermore, the error decay of both QMC methods become very low past $N_r = 1000$ regardless of the stochastic dimension M (see also [14]).

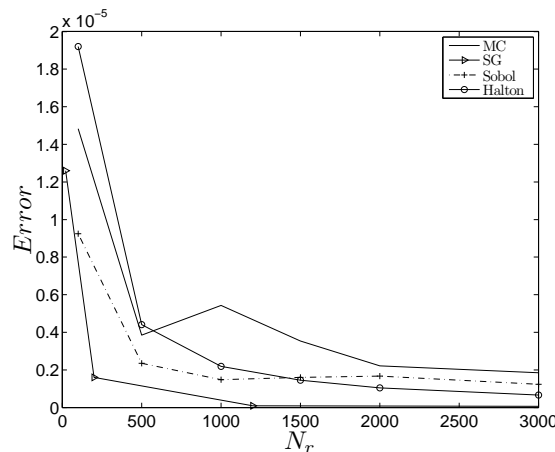


Figure 6: Error (on L^2 norm) of the variance with respect to the number of realizations: SG , QMC , and MC with Halton and Sobol sequences. The reference solution is the truncated solution p_M with $M=10$.

Fig. 6 depicts the convergence of SG and QMC in the absence of truncation error by considering p_M with $M=10$ as the reference solution. In order to establish connections with previous works, we also include the variance error of MC . In SG the number of realizations varies with $K_{SG} = 2, \dots, 5$. The lower error magnitudes with respect to Fig. 5 confirm that the truncation error is the most significant part of the total error. The convergence of SG is faster than QMC and MC , which is consistent with [6, 12]. In fact, the truncated operator (6.8) renders the input data smoother than in the target problem.

6.2 Five-Spot problem

We now consider the classical five-spot problem. The domain has no-flow boundaries at the four sides, and consists of one injection well at the lower left corner and one pumping well at the upper right corner (see Fig. 7). The source and sink terms have strengths $+1$ and -1 , respectively, and are approximated by uniformly distributed loads over the corner elements [7]. The uniqueness of the Neumann problem is ensured by enforcing a zero mean pressure through a penalty formulation [5].

The statistics of the log conductivity is a Gaussian process with power-law covariance

$$C_Y(\mathbf{x}, \mathbf{y}) = \frac{\sigma_Y^2}{|\mathbf{x} - \mathbf{y}|^\beta}, \quad \text{or} \quad C_Y(r) = \sigma_Y^2 r^{-\beta}, \quad (6.10)$$

with $\sigma_Y^2 = 1$ and Hurst exponent $\beta = 0.5$. Moreover, the power-law covariance admits a singularity at short distances, and a cut off is employed to regularize the fractal random field in a sufficiently small lag distance [5].

We consider an unstructured mesh with 945 nodes and 1728 triangular elements, which was generated with the open-source code triangle [27]. A reference solution for

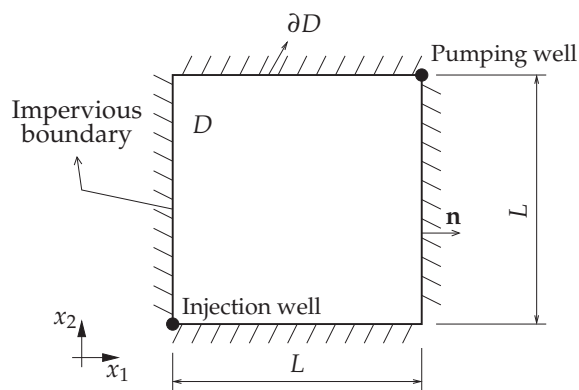


Figure 7: Geometry and boundary conditions for the five-spot problem.

the purpose of comparing the accuracy of the QMC and SG methods is computed by the Monte Carlo method. To numerically illustrate the statistical convergence of the Monte Carlo method, we define the relative error of head variance as

$$E_{rel}(N_r) = \frac{\|\sigma_p^2(N_r) - \sigma_p^2(N_r + 1)\|}{\|\sigma_p^2(N_r + 1)\|}, \tag{6.11}$$

where $\sigma_p^2(N_r)$ denotes the variance of N_r samples generated by the Monte Carlo method based on the expansion (3.1), which was computed by a piecewise-constant finite element approximation of the Fredholm integral equation (3.2). We chose as the reference solution the Monte Carlo solution with 20000 realizations, which lies in an interval where the fluctuation of the relative error is below 10^{-3} (Fig. 8).

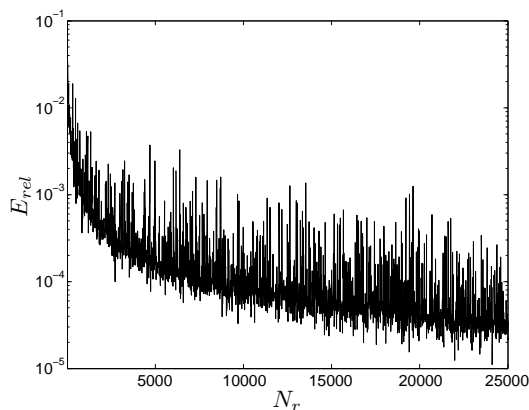


Figure 8: Fluctuation of the relative error (6.11) of the pressure head variance

Fig. 9 shows the mean and variance of this reference solution. The variation of potential is maximum near the top of the flow boundary and minimum elsewhere due to the nature of flow.

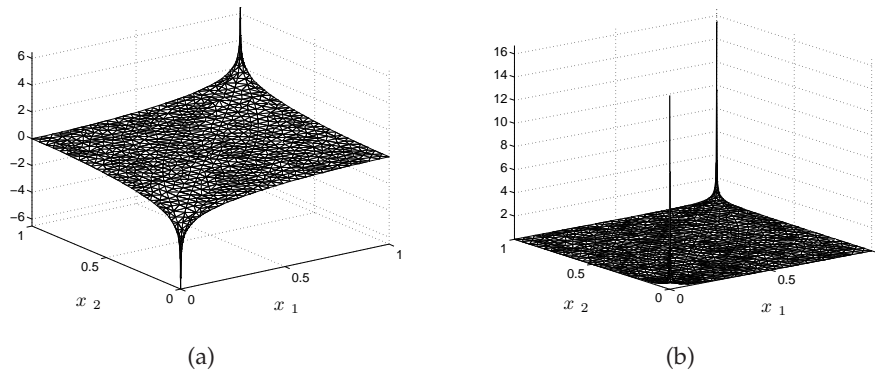


Figure 9: Mean (a) and variance (b) of Monte-Carlo solution of the five-spot problem.

As in Figs. 2-3, we compute QMC solutions with Halton and Sobol sequences considering $M = 10, 100, 400$ and the Smolyak sparse grid algorithm with $K_{SG} = 2, 3, 4$. Comparisons of the pressure variance profiles derived from Monte Carlo simulations (MC) and the QMC for $N_r = 100$ and 1000 are illustrated in Fig. 10 and between profiles from MC and SG by Fig. 11 using semi-log scale. By comparing the variance profiles of Figs. 2 and

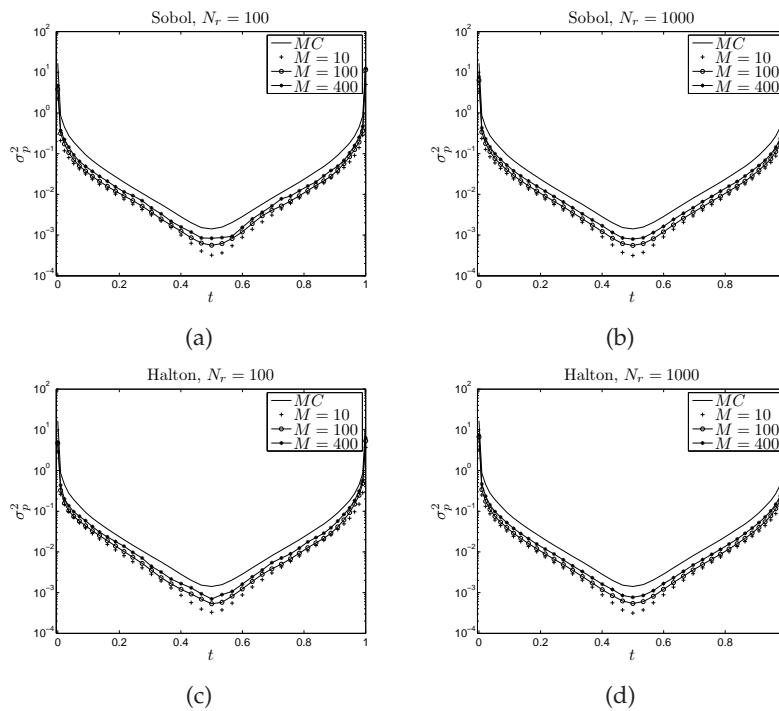


Figure 10: Cross sections of pressure head variance along the line $(x_1, x_2) = (t, t)$ for QMC with Sobol and Halton sequences.

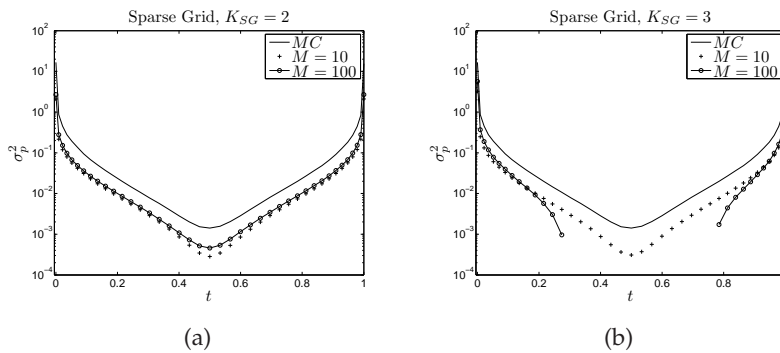


Figure 11: Cross sections of pressure head variance along the line $(x_1, x_2) = (t, t)$ for SG.

10, we notice that the convergence of the QMC methods is faster in the five-spot problem (which has a smoother source term) than in the lognormal pressure head problem. This is consistent with the fact that smoother integrands enhance the convergence of QMC methods [20,22]. In Fig. 11(b) there are missing points in the curve for $M = 100$ because of negative values of variance. These spurious values have also been reported in [28] and are present because the Smolyak quadrature may produce negative weights [13].

As done in the previous experiments, we present in Fig. 12 the error on norm L^2 of the head variance of QMC and SG solutions with respect to the number of realizations N_r . Again the variance error of QMC slowly decreases for $N_r > 1000$. On the other hand, the SG solution for $K_{SG} = 2$ initially seems to converge to the reference solution, but for higher values of M it comes closer to the SG solutions with $K_{SG} = 3, 4$.

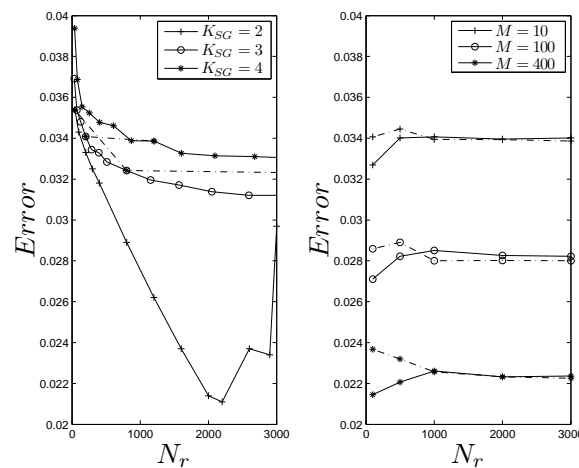


Figure 12: Error (on L^2 norm) of the variance with respect to the number of realizations. Left: SG (dashed lines connect variance errors with $M=10$ and with $M=20$); Right: QMC with Halton (solid lines) and Sobol (dashed lines) sequences.

7 Conclusions

In this study, we compared the solution accuracy and computational cost of *QMC* and *SG* methods, based on Karhunen-Loève decomposition, for saturated flow in randomly heterogeneous porous media. *QMC* methods resort to low discrepancy sequences to generate their realizations, whereas *SG* are built upon algorithms for high-order and high-dimensional polynomial interpolation with a reduced number of collocation points. Both methods generate uncoupled systems of equations, similarly to MC.

We considered two examples of steady state flow in a two-dimensional rectangular domain. In the first example, a random source term is chosen so that the exact solution is a lognormal field with separable, exponential covariance. The second example is a five-spot problem in which the covariance of the log-conductivity is fractal.

In this study, *QMC* seems to be the best choice for experiments with a small number of realizations. The simulation of highly heterogeneous and/or nonlinear problems may need a large ($N_r > 1000$) number of realizations if the user requires a low error tolerance. In these cases it is worth considering *SG* methods, in particular some variants that allow the use of higher stochastic dimensions, such as adaptive sparse grids [11, 18].

Regarding the stochastic dimension, *QMC* managed to perform well for $M \geq 100$, which supports the use of *QMC* on problems with high-dimensional input (see a discussion on this issue in [33]). In the absence of truncation error, the results were consistent with [6] in the sense that *SG* had the best performance for a low dimensional, smooth integrand. Furthermore, the truncation error can significantly contribute to the total error, which makes this a promising field for theoretical contributions such as [23, Sec. 3.2].

The setting of the numerical experiments presented herein have limited the analysis of *QMC* methods to the KL decomposition in contrast with [14], where the efficiency of *QMC* has a sharper picture. On the other hand, the KL decomposition allows for a more detailed study of the errors, in particular the separation of truncation and spatial discretization errors [23]. The results of both [14] and the present work provide insight for a comprehensive error analysis that takes into account the full potential of *QMC* methods.

Although all numerical examples presented in this paper take into account independent and identically distributed variables, the models developed in this study are also applied to condition variables. The latter could be obtained either from Gaussian conditioning kriging [25] or through of Markov Chain Monte Carlo methods [1].

References

- [1] C. Andrieu, N. Freitas, and A. Doucet. An Introduction to MCMC for Machine Learning. *Machine Learning*, 50(1-2):5–43, 2003.
- [2] I. Babuška, F. Nobile, and R. Tempone. A stochastic collocation method for elliptic partial differential equations with random input data. *SIAM J. Numer. Anal.*, 45(3):1005–1034, 2007.
- [3] I. Babuška, R. Tempone, and R. E. Zouraris. Galerkin finite element approximations of stochastic elliptic partial differential equations. *SIAM J. Numer. Anal.*, 42(2):800–825, 2004.

- [4] V. Barthelmann, E. Novak, and K. Ritter. High dimensional polynomial interpolation on sparse grids. *Adv. Comput. Math.*, 12(4):273–288, 2000.
- [5] M. R. Borges, M. A. Murad, F. Pereira, and F. Furtado. A new multiscale scheme for computing statistical moments in single phase flow in heterogeneous porous media. *Adv. Water Resour.*, 32(3):361–382, 2009.
- [6] H.-J. Bungartz and S. Dirnstorfer. Multivariate quadrature on adaptive sparse grids. *Computing*, 71(1):89–114, 2003.
- [7] M. R. Correa and A. F. D. Loula. Unconditionally stable mixed finite element methods for Darcy flow. *Comput. Methods Appl. Mech. Engrg.*, 197(17-18):1525–1540, 2008.
- [8] M. Drmota and R. F. Tichy. Sequences, discrepancies and applications. *Lecture Notes in Mathematics*. Springer, Berlin, 1997.
- [9] J. Galvis and M. Sarkis. Approximating infinity-dimensional stochastic Darcy’s equations without uniform ellipticity. *SIAM J. Numer. Anal.*, 47(5):3624–3651, 2009.
- [10] B. Ganapathysubramanian and N. Zabararas. Sparse grid collocation schemes for stochastic natural convection problems. *J. Comput. Phys.*, 225(1):652–685, 2007.
- [11] T. Gerstner and M. Griebel. Dimension-adaptive tensor-product quadrature. *Computing*, 71(1):65–87, 2003.
- [12] T. Gerstner, M. Griebel, and M. Holtz. Efficient deterministic numerical simulation of stochastic asset-liability management models in life insurance. *Insurance: Mathematics and Economics*, 44(3):434–446, 2009.
- [13] T. Gerstner and M. Griebel. Numerical integration using sparse grids. *Numer. Algorithms*, 18:209–232, 1988.
- [14] I. G. Graham, F. Y. Kuo, D. Nuyens, R. Scheichl, and I. H. Sloan. Quasi-Monte Carlo methods for elliptic PDEs with random coefficients and applications. *J. Comput. Phys.*, 230(10):3668–3694, 2010.
- [15] F. Heiss and V. Winschel. Likelihood approximation by numerical integration on sparse grids. *Journal of Econometrics*, 144(1):62–80, 2008.
- [16] H. Holden, B. Øksendal, J. Ubøe, and T. Zhang. *Stochastic Partial Differential Equations: A Modeling White Noise Functional Approach*. Birkhäuser, 1996.
- [17] L. Kuipers and H. Niederreiter. *Uniform distribution of sequences*. Dover, New York, 1995.
- [18] X. Ma and N. Zabararas. An adaptive high-dimensional stochastic model representation technique for the solution of stochastic partial differential equations. *J. Comput. Phys.*, 229(10):3884–3915, 2010.
- [19] W. J. Morokoff and R. E. Caflisch. Quasi-random sequences and their discrepancies. *SIAM J. Sci. Comput.*, 15(6):1251–1279, 1994.
- [20] W. J. Morokoff and R. E. Caflisch. Quasi-Monte Carlo integration. *J. Comput. Phys.*, 122(2):218–230, 1995.
- [21] H. Niederreiter. Quasi-Monte Carlo methods and pseudo-random numbers. *Bull. Amer. Math. Soc.*, 84(6):957–1041, 1978.
- [22] H. Niederreiter. *Random number generation and quasi-Monte Carlo methods*. SIAM, Philadelphia, 1992.
- [23] F. Nobile, R. Tempone, and C. G. Webster. A sparse grid stochastic collocation method for partial differential equations with random input data. *SIAM J. Numer. Anal.*, 46(5):2309–2345, 2008.
- [24] E. Novak and K. Ritter. The curse of dimension and a universal method for numerical integration. In G. Nürnberger, J. W. Schmidt, and G. Walz, editors, *Multivariate Approximation and Splines*, pages 177–188. Birkhäuser, 1997.

- [25] M. Ravalec, B. Noetinger, and L. Hu. The FFT Moving Average (FFT-MA) Generator: An Efficient Numerical Method for Generating and Conditioning Gaussian Simulations. *Mathematical Geology*, 32(6):701–723, 2000.
- [26] R. Schürer. A comparison between (quasi-)Monte Carlo and cubature rule based methods for solving high-dimensional integration problems. *Math. Comput. Simul.*, 62(3-6):509–517, 2003.
- [27] J. R. Shewchuk. Triangle: Engineering a 2D Quality Mesh Generator and Delaunay Triangulator. In M. C. Lin and D. Manocha, editors, *Applied Computational Geometry: Towards Geometric Engineering*, volume 1148 of *Lecture Notes in Computer Science*, pages 203–222. Springer-Verlag, 1996.
- [28] P. Tsuji, D. Xiu, and L. Ying. Fast method for high-frequency acoustic scattering from random scatterers. *Int. J. Uncertain Quantification*, 1(2):99–117, 2011.
- [29] B. Tuffin. Randomization of Quasi-Monte Carlo Methods for Error Estimation: Survey and Normal Approximation. *Monte Carlo Methods and Applications*, 10(3-4):617–628, 2004.
- [30] D. Xiu. Fast Numerical Methods for Stochastic Computations: A Review. *Commun. Comput. Phys.*, 5(2-4):242–272, 2009.
- [31] D. Xiu and J. Hesthaven. Higher-order collocation methods for differential equations with random inputs. *SIAM J. Sci. Comput.*, 27(3):1118–1139, 2005.
- [32] D. Zhang and Z. Lu. An efficient, high-order perturbation approach for flow in random porous media via Karhunen-Loève and polynomial expansions. *J. Comput. Phys.*, 194(2):773–794, 2004.
- [33] D. Zhang, L. Shi, H. Chang, and J. Yang. A comparative study of numerical approaches to risk assessment of contaminant transport. *Stoch. Environ. Res. Risk Assess.*, 24(7):971–984, 2010.